RESEARCH ARTICLE | SEPTEMBER 26 2023

Influence of the spatial laser energy absorption on the molten pool dynamics in high-power laser beam welding

Xiangmeng Meng ; Stephen Nugraha Putra ; Marcel Bachmann ; Michael Rethmeier

J. Laser Appl. 35, 042024 (2023)
https://doi.org/10.2351/7.0001078

Journal of Laser Applications ARTICLE pubs.aip.org/lia/jla

Influence of the spatial laser energy absorption on the molten pool dynamics in high-power laser beam welding

Cite as: J. Laser Appl. 35, 042024 (2023); doi: 10.2351/7.0001078
Submitted: 16 June 2023 · Accepted: 8 September 2023 ·
Published Online: 26 September 2023

Xiangmeng Meng,[1] Stephen Nugraha Putra,[1] Marcel Bachmann,[1] and Michael Rethmeier[1,2,3]

AFFILIATIONS

[1]BAM Bundesanstalt für Materialforschung und -prüfung, Unter den Eichen 87, Berlin 12205, Germany
[2]Technical University Berlin, Institute of Machine Tools and Factory Management, Pascalstraße 8-9, Berlin 10587, Germany
[3]Fraunhofer Institute for Production Systems and Design Technology, Pascalstraße 8-9, Berlin 10587, Germany

Note: Paper published as part of the special topic on Proceedings of the International Congress of Applications of Lasers & Electro-Optics 2023.

ABSTRACT

The spatial laser energy absorption inside the keyhole is decisive for the dynamic molten pool behaviors and the resultant weld properties in high-power laser beam welding (LBW). In this paper, a numerical simulation of the LBW process, considering the 3D transient heat transfer, fluid flow, and keyhole dynamics, is implemented, in which the free surface is tracked by the volume-of-fluid algorithm. The underlying laser-material interactions, i.e., the multiple reflections and Fresnel absorption, are considered by an advanced ray-tracing method based on a localized level-set strategy and a temperature-dependent absorption coefficient. The laser energy absorption is analyzed from a time-averaged point of view for a better statistical representation. It is found for the first time that a significant drop in the time-averaged laser energy absorption occurs at the focus position of the laser beam and that the rest of the keyhole region has relatively homogeneous absorbed energy. This unique absorption pattern may lead to a certain keyhole instability and have a strong correlation with the detrimental bulging and narrowing phenomena in the molten pool. The influence of different focus positions of the laser beam on the keyhole dynamics and molten pool profile is also analyzed. The obtained numerical results are compared with experimental measurements to ensure the validity of the proposed model.

Key words: laser beam welding, laser energy absorption, molten pool, keyhole dynamics, numerical modeling

I. INTRODUCTION

High-power laser beam welding (LBW) which is performed in the so-called keyhole mode is one of the most utilized joining techniques in industrial applications.[1] Due to the severe evaporation caused by the irradiation of the laser beam with extremely high energy density, the formation of a narrow and deep keyhole inside the molten pool is the most important characteristic of the high-power LBW. Multiple reflections occur on the keyhole wall, and correspondingly the laser energy is partially absorbed at each reflection point. The spatially distributed laser energy which evolutes also dynamically with the keyhole geometry is the initial physical factor for all the subsequent thermo-physical, chemical, and metallurgical behaviors in the molten pool, which determine the final properties of a weld. It is, therefore, of great importance to obtain physical insight into the laser absorption behaviors during LBW.

By far, it is still not technically possible to directly measure the spatial laser energy absorption by an experimental approach. A few investigations can be found, in which the geometry of the keyhole is reconstructed by using high-speed imaging[2] or x-ray transmission,[3,4] and then an offline ray-tracing simulation is performed to obtain the laser energy distribution at a specific time. Matti *et al.* reconstructed the 3D topology of the keyhole front wall based on the image greyscale and a cavity model. The post ray-tracing calculation revealed that the illuminated keyhole front wall

keeps the absorptivity within a range of 35%–43%. X-ray transmissions were performed by Fetzer *et al.*[2] and Allen *et al.*[3] for a 3D reconstruction of the whole keyhole. The local energy distribution and the overall absorptivity were studied using a post-modeled ray-tracing simulation.

With the improvement of hardware and software, the computational fluid dynamics (CFD) model coupled with a free surface tracking algorithm was considered as an effective way to study the relevant physical phenomena, i.e., keyhole dynamics and liquid metal flow, in LBW. With the help of a physics-based model for beam propagation and laser-material interaction, the temporal and spatial distribution of the absorbed laser energy can be calculated, and the correlation between the keyhole topology and the energy distribution can be investigated. The commonly used methodologies include the ray-tracing method,[5] radiative transport equation,[6] and electromagnetic wave equations.[7] The numerical results show that the inclination angle of the keyhole front wall which determines the incident angle of the laser beam plays a critical role in the distribution of the absorbed laser energy.[8] The distribution shows some randomness or irregularity when the keyhole is vertical. In contrast, a relatively uniform distribution can be found with an inclined keyhole front wall. Further numerical studies suggest that the protrusion with micrometer size on the keyhole front wall is decisive for the transient energy distribution. The formation and movement of the small protrusions may initiate the fluctuation and collapse of the keyhole.[9,10]

However, all the analyses in the above-mentioned experimental measurements and numerical calculations focus on the energy distribution at a specific time point or its evolution within a narrow time range of several microseconds. Since the welding process is usually conducted in a time scale of seconds, an instantaneous distribution of the laser energy can easily be influenced by subjective choice and may not guarantee statistical representativity. In this paper, the laser-keyhole interactions, keyhole dynamics, and the molten pool behaviors are studied numerically using a 3D transient CFD model coupled with an advanced ray-tracing algorithm and laser absorption model. The spatial laser energy distribution is analyzed from time-averaged aspects for a better statistical representation. The influences of focus position on the laser energy distribution, keyhole stability, and molten pool behavior are studied.

II. METHODOLOGIES

A. Experimental setup and characterization

AISI 304 stainless steel plates with dimensions of $200 \times 60 \times 10\ \text{mm}^3$ were used as the base metal. Bead-on-plate welding was performed with a Trumpf disk laser system with a maximum output power of 16 kW. The wavelength of the laser beam was 1030 nm, and the focal diameter was 0.42 mm. During the welding experiment, the laser beam irradiated vertically on the workpiece with a focus position of −3 mm. Mechanical cleaning was performed before the welding to remove the oxidation layer to minimize the formation of metallurgical porosity.

Metallographic cross sections were mechanically cut from the specimens and subsequently ground, polished, and etched with a V2A etchant (100 ml H_2O, 100 ml HNO_3, and 10 ml HCl) for the observation of the fusion zone profile by using an optical microscope.

B. Mathematical modeling

In this study, a three-dimensional thermal-fluid flow model coupled with a volume-of-fluid (VOF) algorithm is developed based on the works of the authors[11,12] to calculate the laser-material interaction, keyhole dynamics, and molten pool behavior. The liquid phase is assumed as an incompressible Newtonian fluid with a laminar flow. A brief description of the theoretical framework is given below.

The continuity equation and the Navier–Stokes equation are solved to calculate the fluid flow in the molten pool,

$$\nabla \cdot \mathbf{v} = 0, \tag{1}$$

$$\rho\left(\frac{\partial \mathbf{v}}{\partial t} + (\mathbf{v}\cdot\nabla)\mathbf{v}\right) = -\nabla p + \mu\nabla^2\mathbf{v} - \mu K\mathbf{v} + \mathbf{S_m} + \mathbf{F}, \tag{2}$$

where $\mathbf{v}$ is the velocity, t is the time, ρ is the density, p is the pressure, μ is the dynamic viscosity, and K is the velocity deceleration coefficient in the mushy zone. $\mathbf{S_m}$ includes gravity and buoyance, which is the physical momentum source term, and $\mathbf{F}$ is the converted volumetric force of the recoil pressure, capillary pressure, and the Marangoni stress.

The heat transfer is governed by the energy equation as follows:

$$\rho\left[\frac{\partial h}{\partial t} + (\mathbf{v}\cdot\nabla)h\right] = \nabla\cdot(k\nabla T) + Q, \tag{3}$$

where k is the thermal conductivity and T is the temperature, h is the enthalpy. Q is the numerically converted volumetric heat from the surface heat flux including both laser irradiation and thermal dissipation.

The dynamic free surface of the keyhole and molten pool is traced using the VOF method,[13]

$$\frac{\partial f}{\partial t} + \nabla\cdot(\mathbf{v}f) = 0, \tag{4}$$

where f is the volume fraction. The free surface is located at the cells with a volume fraction between 0 and 1, which implies that no real sharp interface is directly available from the VOF method. The typical momentum and thermal terms which should be in principle applied as boundary conditions need to be converted into volumetric source terms, see $\mathbf{F}$ and Q, by the continuum surface force (CSF) method.[14] The conversion can be achieved by a CSF operator $\tilde{f}$ which can be expressed as

$$\tilde{f} = \frac{2\nabla f[f\rho_{\text{steel}} + (1-f)\rho_{\text{Ar}}]}{(\rho_{\text{steel}} + \rho_{\text{Ar}})}, \tag{5}$$

where ρ_{steel} and ρ_{Ar} are the densities of steel and argon, respectively.

Then the **F** and Q terms can be expanded as

$$\mathbf{F} = \left[p_r(T)\mathbf{n} + \gamma\kappa\mathbf{n} + \frac{\partial\gamma}{\partial T}\frac{\partial T}{\partial \mathbf{s}} \right] \tilde{f}, \tag{6}$$

$$Q = \begin{bmatrix} q_L + q_{\text{vapor}} - h(T - T_0) \\ -\sigma\varepsilon_{\text{r}}(T^4 - T_0^4) - \rho v_{evp}\Delta L_v \end{bmatrix} \tilde{f}. \tag{7}$$

All the relevant physical mechanisms of LBW contribute to the **F** and Q terms. The first, second, and third terms on the right-hand side of Eq. (6) are the recoil pressure, capillary pressure, and the Marangoni stress. $P_{\text{r}}(T)$ *is* a temperature-dependent recoil pressure model, **n** is the unit normal vector of the free surface, γ is the surface tension coefficient, κ is the curvature, and **s** is the tangential vector of the keyhole surface. The five terms on the right-hand side of Eq. (7) are the laser energy input, the secondary heating effect from the high-temperature vapor, and the thermal dissipation due to convection, radiation, and evaporation, respectively, where h_{c} is the convective heat loss coefficient, T_0 is the room temperature, σ is the Stefan–Boltzmann constant, ε_{r} is the emissivity, and v_{evp} is the free surface recession speed due to evaporation.

The evaporation-induced recoil term is the key driving force to sustain an opening keyhole, which can be written as[15]

$$p_r(T) = \frac{AB}{\sqrt{T}} \exp\left(-\frac{m\Delta L_v}{R_g T} \right). \tag{8}$$

Here, A and B are material-dependent evaporation coefficients, which are taken as 0.55 $\text{K}^{1/2}$ and 3.9×10^{12} kg/m s^2 for pure iron, respectively; m is the molar mass, ΔL_{v} is the evaporation latent heat, R_{g} is the ideal gas constant.

As discussed above, a physical description of the beam propagation and the laser-material interaction is the fundamental basis for laser energy absorption. In this study, a ray-tracing algorithm was established to calculate the multiple reflections inside the keyhole. To improve the accuracy of the calculated reflection path, a localized level-set algorithm is integrated into the ray-tracing method,[16] which is only executed within the free surface cells rather than the whole simulation domain, so that no further computational intensity is introduced. Additionally, a novel Fresnel absorption model is applied, in which the absorptivity is not only a function of the incident angle but also the laser characteristics, surface temperature, and material properties.[17] The absorption model requires, therefore, no adaption of any empirical parameters. More details about the absorption model can be found in the supplementary material.[23] The absorption coefficient of 304 stainless steel for a 1030 nm disk laser at different temperatures is plotted in Fig. 1. The dashed line shows the absorptivity from the commonly used absorption model with empirically determined parameters, such as in the work of Refs. 5 and 6. The solid lines represent the calculated absorptivities at different temperatures. In general, the absorptivity increases with the temperature, and the new model provides a more moderate absorption compared with the empirical model.

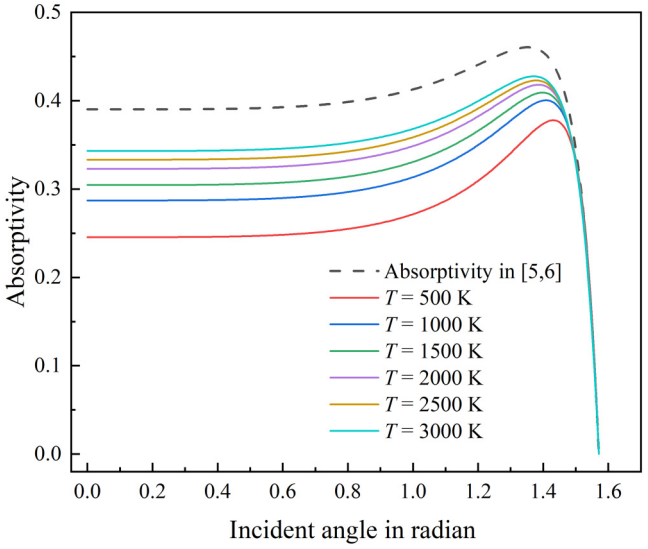

FIG. 1. Absorptivity of the laser under different temperatures.

The evolution of the spatial laser energy distribution, keyhole dynamics, and thermo-fluid flow can be calculated by the numerical model. The time-average and root-mean-square error (RMSE) operations are conducted to the laser energy absorption during simulation so that statistical analysis can be achieved.

The computational domain has dimensions of $30 \times 8 \times 12$ mm^3 and is meshed to accommodate a solid steel phase of thickness 10 mm and a gaseous Ar phase of thickness 2 mm. The central region is uniformly meshed using 0.2 mm hexahedron cells, and the cell size grows gradually in the zone far away from the molten pool. The universal CFD software ANSYS Fluent 21.2 is used to solve the transport equations and VOF equation, with the convection-diffusion equations spatially discretized via the second-order upwind method. The pressure implicit with splitting of operators (PISO) algorithm was utilized for the pressure-velocity coupling. The important temperature-dependent material properties are plotted in Fig. 2. More detailed description of the boundary conditions, numerical algorithms, and model parameters can be found in the authors' previous works.[18]

III. RESULTS AND DISCUSSION

The accuracy of the applied model has been well validated in a wide range of laser power with multiple types of metallic materials.[11,12,18,19] Figure 3 shows a representative comparison of the fusion lines from numerical modeling and experiment with the selected welding parameters in this paper, i.e., the laser power of 4 kW, welding speed of 1 m/min, and focus position of −3 mm, in which good agreement with an error less than 10% in the penetration depth can be confirmed. It should be noted that the metal accumulation above the workpiece surface and the porosity currently cannot be reproduced numerically due to the ignorance of

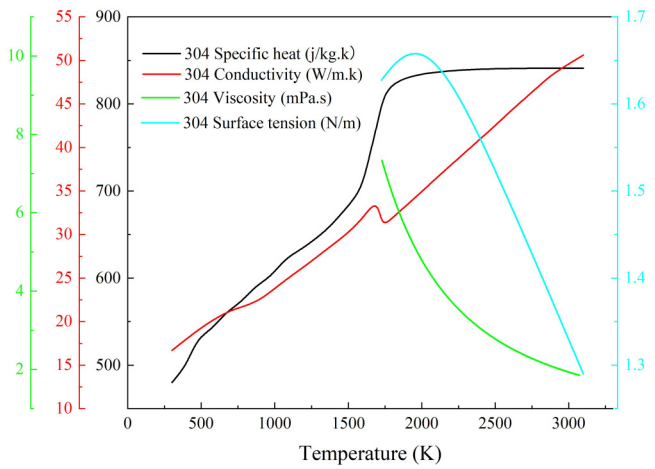

FIG. 2. Temperature-dependent material properties of 304 steel.

some physics in the model, such as the thermal deformation of the solid metal and the interaction between bubbles and the liquid metal. These effects should, however, have no influence on the keyhole dynamics and the laser absorption.

The dynamic distribution of the absorbed laser energy on the keyhole wall is given in Fig. 4. An apparent necking phenomenon occurs at the keyhole opening region at the time of t_0 in Fig. 4(a), and most of the dynamic laser energy is consequently absorbed

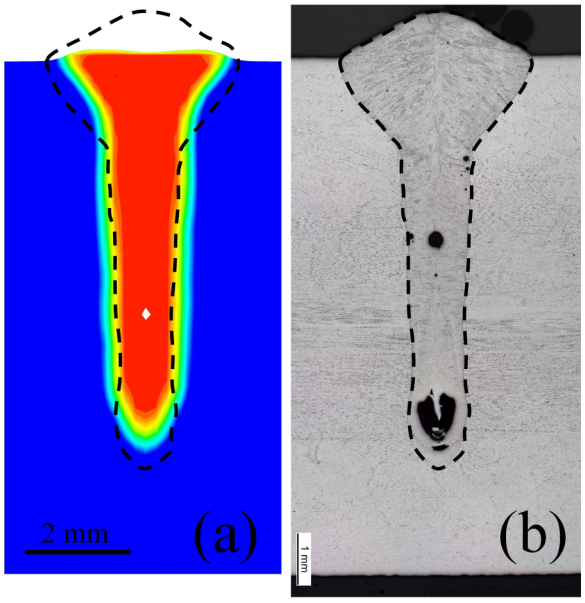

FIG. 3. Comparison of the calculated and experimental cross-sections (4 kW, 1 m/min, −3 mm): (a) simulation result, the red color corresponds to the fusion zone. (b) Experimental results.

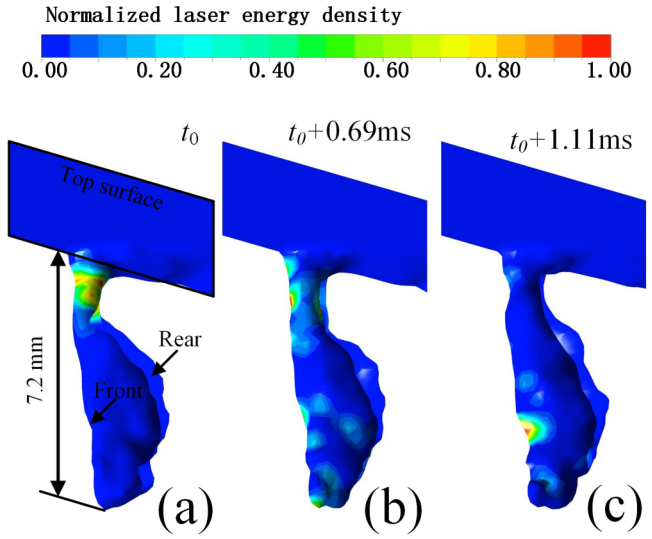

FIG. 4. Transient evolution of the absorbed laser energy on the keyhole surface: (a) at t_0 with the maximum value of 9.3×10^8 W/m^2, (b) at $t_0 + 0.69$ ms with the maximum value of 5.7×10^8 W/m^2, (a) at $t_0 + 1.11$ ms with the maximum value of 17.2×10^8 W/m^2.

there. After several hundred microseconds (at $t_0 + 0.69$ ms), the necking part is reopened by the recoil pressure, and the laser energy shows a quite irregular distribution on the keyhole front wall which has a relatively smooth geometry, see Fig. 4(b). At the time of $t_0 + 1.11$ ms, a protrusion forms on the keyhole front wall,

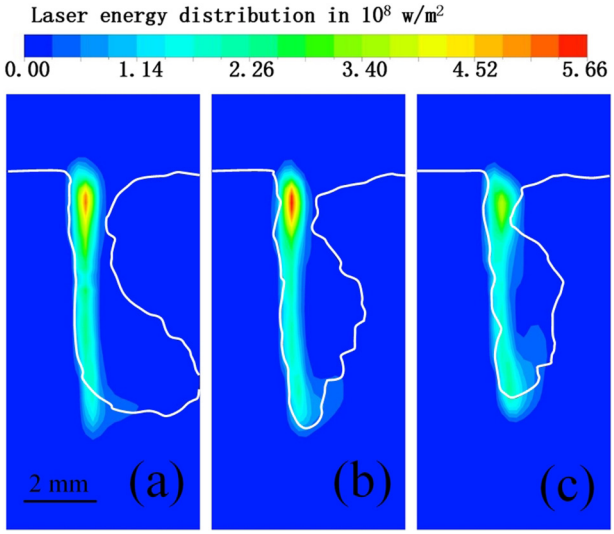

FIG. 5. Time-averaged laser energy distribution (within 200 ms) along the longitudinal section for different focus positions: (a) −3 mm, (b) 0 mm, (c) 3 mm.

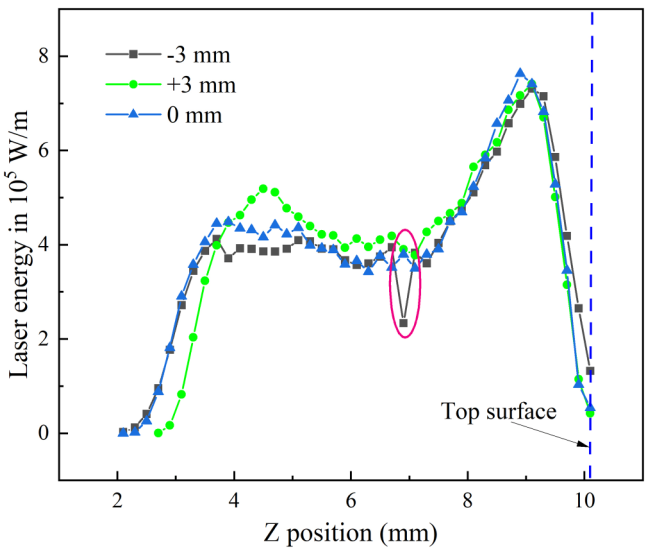

FIG. 6. Time-averaged laser energy distribution (within 200 ms) along the thickness direction.

and its top surface is under the direct irradiation of the laser beam, which leads to a localized spot with an extremely high energy density of 17.2×10^8 W/m^2. In comparison, the maximum energy densities in Figs. 4(a) and 4(b) are only 9.3×10^8 and 5.7×10^8 W/m^2, respectively. It is usually considered that the energy density of the laser beam should reach 10^6 W/cm^2 (10^{10} W/m^2) to reach the keyhole mode. However, the absorption of the laser energy depends not only on the incident angle but also on the temperature, see Fig. 1. The absorbed laser energy on the keyhole surface can be one order of magnitude lower than the original laser energy, considering the absorptivity of 20%–30%.

These three typical distribution regimes have also been found in other numerical works.[8–10,20] However, it is also recognized that their occurrence shows high randomness. Within a timeframe of microseconds, one type can convert into another one without any identifiable periodic evolution. It implies that no energy distribution at a certain time point or within a short range of time can provide sufficient statistical representability.

Therefore, the spatial energy distribution is analyzed from a time-averaged point of view in this study, as shown in Fig. 5. It should be noted that the white lines in the figure are the keyhole profile at a specific time, providing a better intuition for the locations. Compared with the scattered and concentrated dynamic energy distribution in Fig. 4, the time-averaged laser energy represents a homogeneous distribution. Most of the laser energy is absorbed in a region near the keyhole wall rather than exactly on it. It implies that the formed protrusions play a dominant role in the absorption of the laser energy, corresponding to the distribution in Fig. 4(c), which is consistent with the work from Refs. 9 and 10.

Due to the fluctuation of the keyhole opening, more energy is absorbed in the upper part. In the deep-penetration region, a relatively uniform distribution is observed. Figure 6 shows the time-averaged absorbed laser power per length (in W/m) along the thickness direction. Three characteristic regions can be clarified, namely, a top region with high energy absorption, a stable absorption region that produces the feature of deep penetration, and a bottom region where the absorbed energy drops dramatically. From a statistical aspect, the laser beam can hardly reach the keyhole bottom, even for the LBW with low welding speeds (1 m/min in this paper).

More interestingly, an abrupt drop in the energy absorption can be found at the focus position when a negative one is applied, see Figs. 6(a) and 7. It is largely due to the fact that the laser beam has the smallest diameter at the focus position so that it has correspondingly the least possibility to be received by the keyhole surface.

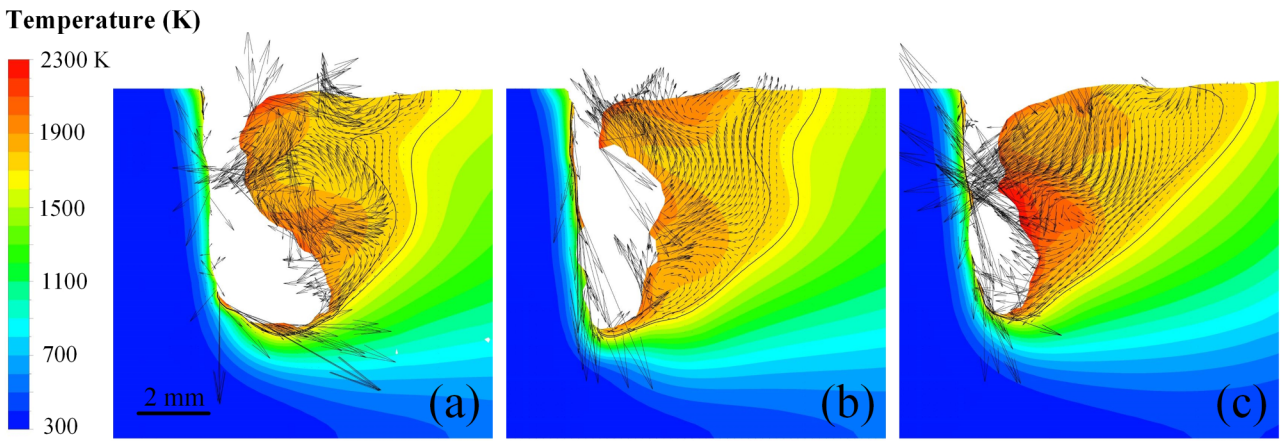

FIG. 7. Molten pool profile and the velocity field with different focus positions: (a) −3 mm, (b) 0 mm, and (c) +3 mm. The black lines correspond to the liquidus and solidus temperatures, respectively.

Figure 7 shows the different molten pool profiles and the velocity field of the liquid metal. Despite the same line energy, the different laser energy distribution resulting from the different focal positions produces a significant variation in the molten pool profile. As a negative focus position is applied, the molten pool is characterized by an upper elongated region and a lower bulging region, between which a narrowing phenomenon can be observed. It is deduced that the reduction of the laser absorption at the focus position contributes to the formation of the narrowing phenomenon. The narrowing and bulging phenomena are mitigated and eventually suppressed as the focus position moves upward. With a focus position of +3 mm, the molten pool shows a regular profile, i.e., a monotonic decrease of molten pool length along the thickness direction.

The unique molten pool shape in Fig. 7(a) has been found to have a strong correlation with the formation of some welding defects, such as hot cracking, porosity, and the inhomogeneous distribution of the filler material.[12,18,21] In the work of Tsukamoto *et al.* with electron beam welding, it is found that the focus position has a decisive impact on the occurrence of the so-called delaying solidification which is caused by the bulging in the molten pool.[22] This delaying solidification may initiate hot-cracking defects. The findings are instructive but not directly applicable to the LBW process due to the different physics involved between the two processes. For example, no multiple reflections occur in the electron beam welding. To the best of our knowledge, this paper provides the first numerical reproduction of the influence of the focus position on the narrowing and bulging phenomena and clarifies its importance. With the application of a positive focus position, the molten pool should have the least susceptivity of hot cracking. It must be noted that a positive focus position may not always bring beneficial effects. Lack of penetration, for instance, can also be produced due to insufficient energy density.

The distribution of the absorbed laser energy also shows a noticeable influence on the keyhole stability, as shown in Fig. 8. For the three welding cases with the same line energy but different focus positions, the possibility of the keyhole collapse position has a similar pattern, namely, two separated collapse groups at bottom and opening. As the focus position changes from +3 to −3 mm, more collapses tend to occur at the opening region of the keyhole (14%–22%). The opening/collapse of the keyhole is determined by the balance between the evaporation-induced recoil pressure and the hydrostatic/hydrodynamic pressure of the liquid metal. With a focus position of −3 mm, two circulations exist in the molten pool, as shown in Fig. 7(a). These two circulations exhibit different flowing directions, but they converge with each other and then flow forward, intending to push the liquid metal against the keyhole's front wall. As the focus position moves upwards, the lower circulation is restrained, resulting in a mitigation of the forward-flowing regime, which will reduce the probability of the upper collapse of the keyhole. Meanwhile, the more frequent collapse at the upper region may also partly be attributed to the drop of the absorbed energy observed at the focus position (Fig. 6). Since the least laser energy is absorbed there, the weakest evaporation, and accordingly, the weakest recoil pressure is generated to maintain the stability of the keyhole, leading to more frequent collapses.

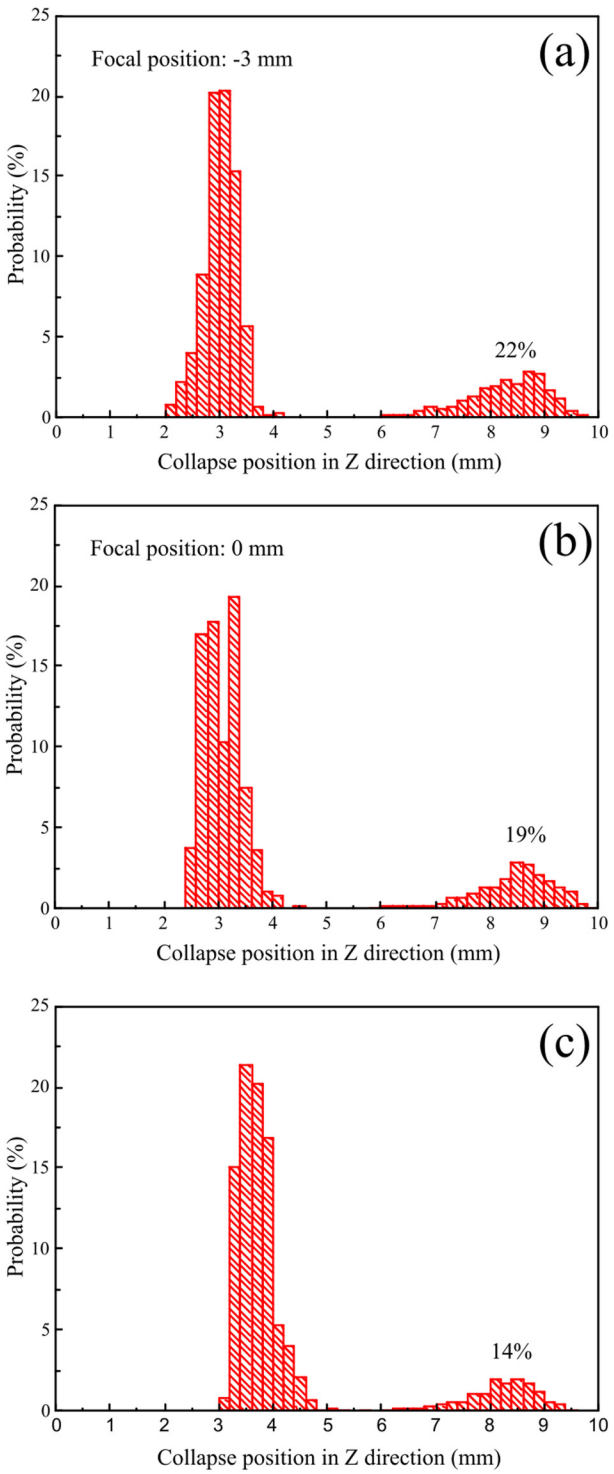

FIG. 8. Possibility of the collapse position of the keyhole (10 mm is the top surface of the workpiece) with different focus positions: (a) −3 mm, (b) 0 mm, and (c) +3 mm.

IV. CONCLUSIONS

In this paper, the spatial laser energy distribution and its influences on the keyhole dynamics and molten pool behaviors are studied, especially from a statistical aspect in a relatively long-time range (several hundred microseconds), using a numerical heat transfer and fluid flow model considering multiple reflections of the laser beam and temperature-dependent absorption. The main conclusions are drawn below.

(1) Several typical distribution regimes can be recognized from the transient evolution of the absorbed laser energy, but a general trend cannot be clarified due to the randomness of their occurrence. In contrast, it is very clear from the time-averaged aspect that more energy is absorbed in the upper part and a relatively uniform distribution is observed in the deep-penetration region.
(2) When the focus position is inside of the workpiece, namely, a negative focus position is applied, an abrupt drop of the time-averaged laser energy absorption can be found at the focal plane. A clear causal correlation between the time-averaged laser absorption and statistical the molten pool dynamics still requires further study.
(3) The focal position shows an important influence on the molten pool profile. As the focus position moves upwards from negative (below the workpiece surface) to positive (above the workpiece surface) in this study, the narrowing and bulging phenomena are mitigated and eventually eliminated.
(4) The variation of the flowing pattern in the molten pool caused by the different focus positions influences the dynamic balance between recoil pressure and the hydrostatic/hydrodynamic pressure of the liquid metal, and correspondingly, results in different keyhole stabilities. The abrupt drop of the time-averaged laser energy absorption may also contribute to the more frequent keyhole collapse at the upper region due to the weakest metal evaporation there.

ACKNOWLEDGMENT

This work was funded by the Deutsche Forschungsgemeinschaft (DFG, German Research Foundation)—Project Nos. 506270597 and 466939224.

AUTHOR DECLARATIONS

Conflict of Interest

We declare that we have no financial and personal relationships with other people or organizations that can inappropriately influence our work. There is no professional or other personal interest of any nature or kind in any product, service, and/or company that could be construed as influencing the position presented in, or the review of, the manuscript.

Author Contributions

Xiangmeng Meng: Formal analysis (lead); Funding acquisition (equal); Investigation (lead); Methodology (lead); Project administration (equal); Supervision (supporting); Validation (lead); Visualization (lead); Writing – original draft (lead); Writing – review & editing (equal). **Stephen Nugraha Putra:** Investigation (supporting); Methodology (equal); Software (equal). **Marcel Bachmann:** Formal analysis (equal); Funding acquisition (equal); Investigation (equal); Project administration (equal); Supervision (equal); Writing – review & editing (equal). **Michael Rethmeier:** Formal analysis (supporting); Investigation (equal); Project administration (supporting); Supervision (equal); Writing – review & editing (equal).

REFERENCES

[1]M. Rethmeier, A. Gumenyuk, and M. Bachmann, "High-power laser beam welding for thick section steels—New perspectives using electromagnetic systems," Sci. Technol. Weld. Join. **27**, 43–51 (2022).
[2]R. S. Matti and A. F. H. Kaplan, "Post-modelling of images from a laser-induced wavy boiling front," Appl. Surf. Sci. **357**, 2277–2284 (2015).
[3]F. Fetzer, C. Hagenlocher, R. Weber, and T. Graf, "Geometry and stability of the capillary during deep-penetration laser welding of AlMgSi at high feed rates," Opt. Laser Technol. **133**, 106562 (2021).
[4]T. R. Allen, W. Huang, J. R. Tanner, W. Tan, J. M. Fraser, and B. J. Simonds, "Energy-coupling mechanisms revealed through simultaneous keyhole depth and absorptance measurements during laser-metal processing," Phys. Rev. Appl. **13**, 064070 (2020).
[5]W.-I. Cho, S.-J. Na, C. Thomy, and F. Vollertsen, "Numerical simulation of molten pool dynamics in high power disk laser welding," J. Mater. Process. Technol. **212**, 262–275 (2012).
[6]A. Otto, H. Koch, K. H. Leitz, and M. Schmidt, "Numerical simulations—A versatile approach for better understanding dynamics in laser material processing," Phys. Proc. **12**, 11–20 (2011).
[7]M. Courtois, M. Carin, P. Le Masson, S. Gaied, and M. Balabane, "A new approach to compute multi-reflections of laser beam in a keyhole for heat transfer and fluid flow modelling in laser welding," J. Phys. D: Appl. Phys. **46**, 505305 (2013).
[8]W. Tan and Y. C. Shin, "Analysis of multi-phase interaction and its effects on keyhole dynamics with a multi-physics numerical model," J. Phys. D: Appl. Phys. **47**, 345501 (2014).
[9]Y. Wang, P. Jiang, J. Zhao, and S. Geng, "Effects of energy density attenuation on the stability of keyhole and molten pool during deep penetration laser welding process: A combined numerical and experimental study," Int. J. Heat Mass Transfer **176**, 121410 (2021).
[10]C. Zhao, Q. Guo, X. Li, N. Parab, K. Fezzaa, W. Tan, and T. Sun, "Bulk-explosion-induced metal spattering during laser processing," Phys. Rev. X **9**, 021052 (2019).
[11]X. Meng, M. Bachmann, A. Artinov, and M. Rethmeier, "The influence of magnetic field orientation on metal mixing in electromagnetic stirring enhanced wire feed laser beam welding," J. Mater. Process. Technol. **294**, 117135 (2021).
[12]X. Meng, A. Artinov, M. Bachmann, Ö Üstündağ, A. Gumenyuk, and M. Rethmeier, "The detrimental molten pool narrowing phenomenon in wire feed laser beam welding and its suppression by magnetohydrodynamic technique," Int. J. Heat Mass Transfer **193**, 122913 (2022).
[13]C. W. Hirt and B. D. Nichols, "Volume of fluid (VOF) method for the dynamics of free boundaries," J. Comput. Phys. **39**, 201–225 (1981).
[14]J. U. Brackbill, D. B. Kothe, and C. Zemach, "A continuum method for modeling surface tension," J. Comput. Phys. **100**, 335–354 (1992).
[15]V. Semak and A. Matsunawa, "The role of recoil pressure in energy balance during laser materials processing," J. Phys. D: Appl. Phys. **30**, 2541–2552 (1997).
[16]X. Meng, S. N. Putra, M. Bachmann, A. Artinov, and M. Rethmeier, "Influence of the free surface reconstruction on the spatial laser energy

distribution in high power laser beam welding modeling," J. Laser Appl. **34**, 042023 (2022).
[17]Z. Yang, A. Bauereiß, M. Markl, and C. Körner, "Modeling laser beam absorption of metal alloys at high temperatures for selective laser melting," Adv. Eng. Mater. **23**, 2100137 (2021).
[18]X. Meng, M. Bachmann, A. Artinov, and M. Rethmeier, "A study of the magnetohydrodynamic effect on keyhole dynamics and defect mitigation in laser beam welding," J. Mater. Process. Technol. **307**, 117636 (2022).
[19]Y. Fan, X. Meng, M. Bachmann, A. Artinov, and M. Rethmeier, "Numerical analysis of the influence of an auxiliary oscillating magnetic field on suppressing the porosity formation in deep penetration laser beam welding of aluminum alloys," in *Proceedings of The 13th International Seminar Numerical Analysis of Weldability, Graz, Austria* (Verlag der Technischen Universität Graz, Graz, Austria, 2022).
[20]S. A. Khairallah, T. Sun, and B. J. Simonds, "Onset of periodic oscillations as a precursor of a transition to pore-generating turbulence in laser melting," Addit. Manuf. Lett. **1**, 100002 (2021).
[21]A. Artinov, X. Meng, M. Bachmann, and M. Rethmeier, "Study on the transition behavior of the bulging effect during deep penetration laser beam welding," Int. J. Heat Mass Transfer **184**, 122171 (2022).
[22]S. Tsukamoto and H. Irie, "Mechanism of locally delayed solidification in electron beam welding," Weld. Int. **5**, 177–183 (1991).
[23]See the supplementary material online for the description of the laser absorption models..